

Synthesis of Sr-doped LaMnO_3 and LaCrO_3 powders by combustion method: structural characterization and thermodynamic evaluation

(Síntese de pós de LaMnO_3 e LaCrO_3 dopados com Sr pelo método de combustão: caracterização estrutural e avaliação termodinâmica)

A. L. A. da Silva, L. da Conceição, A. M. Rocco, M. M. V. M. Souza

Escola de Química, Universidade Federal do Rio de Janeiro - UFRJ, Centro de Tecnologia, Bloco E, sala 206,
Rio de Janeiro, RJ, Brazil 21941-909
mmattos@eq.ufrj.br

Abstract

Lanthanum strontium manganite (LSM) and chromite (LSC) powders, as well as the corresponding non-doped samples, were synthesized by the combustion method, using two different fuels (urea and glycine). The ignition of the reagent mixture with urea takes a longer time and the maximum temperature is higher than using glycine, for doped samples. The theoretical calculations of exothermic heat and adiabatic flame temperatures indicate favorable conditions for combustion to occur. However, calcination is an essential step for a good crystallization of perovskite phase. X-ray diffraction patterns showed formation of only perovskite phase for the samples synthesized with urea. The crystallite sizes are in the range of 19-25 nm, with smaller values when urea was used as fuel. Scanning electron microscopy showed the presence of agglomerates, formed by fine particles of different shapes. Thermogravimetric analysis revealed that the weight loss is much higher for manganites, with complete burn out of organics at 850-900 °C.

Keywords: perovskites, combustion synthesis, X-ray diffraction, thermogravimetric analysis, microstructure.

Resumo

Manganita de lantânio dopada com estrôncio (LSM) e cromita (LSC) em pó, bem como as correspondentes amostras não dopadas, foram sintetizadas pelo método de combustão, usando dois diferentes combustíveis (ureia e glicina). A ignição da mistura reacional com ureia leva mais tempo e a temperatura máxima é maior do que usando glicina, para as amostras dopadas. Os cálculos teóricos de calor de reação e temperatura de chama adiabática indicam condições favoráveis à combustão. No entanto, a calcinação é uma etapa essencial para uma boa cristalização da fase perovskita. Os padrões de difração de raios X mostraram a formação apenas da fase perovskita para as amostras sintetizadas com ureia. Os tamanhos de cristalitos estão na faixa de 19-25 nm, com valores menores quando a ureia é usada como combustível. Análises de microscopia eletrônica de varredura mostraram a presença de aglomerados, formados por partículas finas de diferentes formas. A análise termogravimétrica revelou que a perda de peso é muito maior para as manganitas, com queima completa dos orgânicos em 850-900 °C.

Palavras-chave: perovskitas, síntese de combustão, difração de raios X, análise termogravimétrica.

INTRODUCTION

Perovskites are mixed ceramic oxides with ABO_3 type crystal structure where cations with a large ionic radius have 12 coordination to oxygen atoms and occupy A-sites, and cations with smaller ionic radius have 6 coordination and occupy B-sites [1]. A and O form a cubic packing and B is contained in the octahedral voids in the packing. The perovskite structure may undergo atomic distortion leading to orthorhombic or rhombohedral unit cells [2]. Perovskites like lanthanum manganite and chromite are interesting materials for application in solid oxide fuel cells (SOFC) due to chemical and thermal stability, mechanical strength and high electrical conductivity [2, 3]. The electrical conductivity of these materials can be enhanced by substituting a lower valence ion, such as Sr, on the La site. Sr-doped LaMnO_3 (LSM) and LaCrO_3 (LSC) are

currently the preferred ceramic materials for cathode and interconnect in the SOFC [3, 4].

Different synthesis methods have been developed for the production of perovskite powders, like solid-state reaction, sol-gel technique, hydrothermal synthesis, coprecipitation, and combustion [5-8]. Combustion synthesis is characterized by fast heating rates, high temperatures and short reaction times [9, 10]. It is a straightforward preparation process to produce homogeneous, very fine, crystalline and unagglomerated multicomponent oxide nanopowders, without intermediate decomposition steps [11]. In the solution combustion synthesis, an aqueous solution of the desired metal salts is heated together with a suitable organic fuel, until the mixture ignites and a fast combustion reaction takes off [9, 12]. Several fuels have been used in the combustion synthesis of perovskites, like glycine, urea, oxalyl-hydrazine, citric acid and sucrose [8,

13-15]. All these fuels serve two purposes: (i) they are the source of C and H, the reducing elements, which form CO₂ and H₂O on combustion and liberate heat; (ii) they form complexes with the metal ions facilitating homogeneous mixing of the cations in solution [9]. The fuels differ in the reducing power, the combustion temperature and the amount of gases they generate, which affects the characteristics of the reaction product [12]. The properties of ceramic materials for electrodes and interconnects in SOFC are extremely dependent on the conditions of powder synthesis, which in turn depend on the nature of the fuel used in the combustion synthesis. Pingbo *et al.* [16] investigated the influence of the glycine/oxidizer ratio on the combustion synthesis of LSM, showing that the crystallite size increases when this ratio decreases, due to an increase in the flame temperature. Mukasyan *et al.* [17] and Deshpande *et al.* [18] showed that the mechanism of combustion synthesis of LSC and the characteristics of the synthesized powders are closely related to the glycine/oxidizer ratio; increasing this ratio the flame temperature increases. The mechanism of combustion synthesis of lanthanum chromite with urea was investigated by Biamino and Badini [19] using thermal analysis and identifying the reaction products by mass spectrometry. To our knowledge, none of the combustion synthesis studies until now reported the effect of the fuel on the structural and morphological properties of LSM or LSC powders.

The aim of this work is to study the influence of the fuel (urea and glycine) used in the combustion synthesis on the flame temperature and ignition time of lanthanum strontium manganite (LSM) and chromite (LSC) powders, as well as the corresponding non-doped samples. Thermodynamic calculations of the adiabatic flame temperatures were performed and compared with experimentally measured temperatures. The combustion synthesized powders were characterized by X-ray diffraction (XRD), scanning electron microscopy (SEM) and thermal analysis (TGA/DTA), analyzing the variation in the powder properties based on the characteristics of combustion reaction.

EXPERIMENTAL

Material synthesis

The materials used in the synthesis were metal nitrates: La(NO₃)₃·6H₂O, Sr(NO₃)₂, Mn(NO₃)₂·6H₂O, Cr(NO₃)₃·9H₂O, and the propellants were urea (CO(NH₂)₂) and glycine (NH₂CH₂COOH). All reagents were from Vetec, Brazil, with 99.9% purity. The samples were synthesized by combustion method, using urea and glycine as fuel agents. The metal nitrates were dissolved with the fuel in distilled water and heated (under stirring) at 80 °C, until the water evaporation and formation of a gel. After that, the gel was introduced in a muffle furnace (EDG 3000 3P), previously heated at 300 °C. Once ignited, the gel underwent a combustion process and yielded a voluminous powder. The ignition time and the flame temperature were measured during the combustion synthesis, with a thermocouple (type K) inserted in the

reagent mixture. The powder was then calcined in flowing air (60 mL.min⁻¹) with a heating rate of 10 °C.min⁻¹ up to 900 °C for 6 h. The amount of fuel used on the preparation of these materials was based on the following equation: $\sum n_i \nu_i = 0$, where n_i is the number of mols of each reagent and ν_i is the number of oxidation, calculated according to the propellant chemistry [20]. The fuel/oxidizer (metal nitrates) ratio was 1, which corresponds to the stoichiometric ratio.

All La_{1-x}Sr_xMnO₃ and La_{1-x}Sr_xCrO₃ powder materials were prepared with nominal composition of $x = 0.3$. The prepared perovskites will be referred to as LMU or LCU (non-doped samples), LSMU or LSCU (doped samples) for those prepared from urea and LMG or LCG, LSMG or LSCG for those derived from glycine route.

Thermodynamic calculations

The enthalpy of combustion reaction can be expressed as:

$$\Delta H_{298}^0 = (\sum n \Delta H_{f,298}^0)_{\text{products}} - (\sum n \Delta H_{f,298}^0)_{\text{reactants}} \quad (\text{A})$$

and

$$\Delta H_{298}^0 = \int_{298}^T (\sum n C_p)_{\text{products}} dT \quad (\text{B})$$

where n is the number of mols of each species, ΔH_f^0 is the enthalpy of formation, C_p is the heat capacity and T is the adiabatic flame temperature. Using the thermodynamic data for reactants and products found in the literature data [21-25], and calculating the C_p of doped perovskites according to the equation [26]:

$$C_{p,\text{perovskites}} = \sum x_i C_{p,\text{binary oxides}} \quad (\text{C})$$

where x_i is the stoichiometric coefficient of the perovskite formation reaction from its binary oxides, it was possible to determine the enthalpy of combustion for each reaction, as well as the adiabatic flame temperatures.

Characterization

X-ray powder diffraction (XRD) patterns were recorded in a Rigaku Miniflex II diffractometer, with CuK α radiation and monochromator, with speed of 2° min⁻¹. The crystallite sizes (D_{XRD}) and microstrain (ϵ) of the calcined samples were calculated using the model proposed by Williamson and Hall [27], by means of the following formula:

$$\beta \frac{\cos\theta}{\lambda} = \frac{1}{D_{\text{XRD}}} + 4\epsilon \frac{\sin\theta}{\lambda} \quad (\text{D})$$

where θ is the diffraction angle, λ is the wavelength of incident radiation and β is the full width at half maximum (FWHM) of the peak. Plotting the $\beta \cos\theta/\lambda$ versus $4\sin\theta/\lambda$ straight line yields the crystallite size from interception with the ordinate and microstrain from the slope. The calculus was done using the FullProf software.

The microstructure of the powders was investigated by scanning electron microscopy (SEM) using Hitachi TM-1000 equipment. The acceleration voltage was 15 kV, using backscattering electron.

Thermogravimetric analysis (TGA) and differential thermal analysis (DTA) of the as-prepared powders were carried out using a TA thermal analyzer (SDT Q600 model) with heating rate of 10 °C min⁻¹ in air flow (50 mL min⁻¹) from room temperature up to 1000 °C.

RESULTS AND DISCUSSION

Time and temperature of combustion reaction

Fig. 1 shows the evolution of temperature as a function of time during the combustion synthesis of LaMnO₃ and LaCrO₃. The ignition of the reagent mixture with urea takes a longer time and the maximum temperature is lower. The combustion process with glycine is more rapid, attaining higher temperature of flame.

The results of combustion temperature for the Sr-doped samples are displayed in Fig. 2. The ignition time using

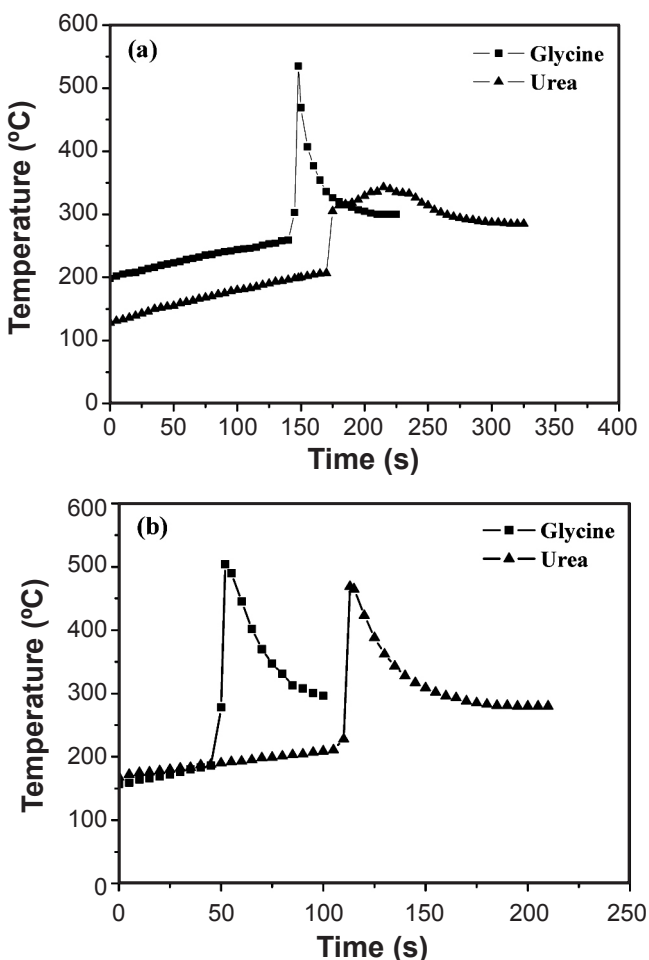


Figure 1: Evolution of temperature as a function of time during combustion synthesis for (a) LaMnO₃ and (b) LaCrO₃ powders. [Figura 1: Evolução da temperatura com o tempo durante a síntese por combustão dos pós de (a) LaMnO₃ e (b) LaCrO₃.]

glycine is faster; however, in the case of doped samples, the maximum temperature is lower than using urea. This behavior shows that urea favors a more complete combustion reaction during the synthesis process, with evolution of a larger amount of gases, which contributes to the formation of materials of high porosity, good crystallinity and nanometric particles [28].

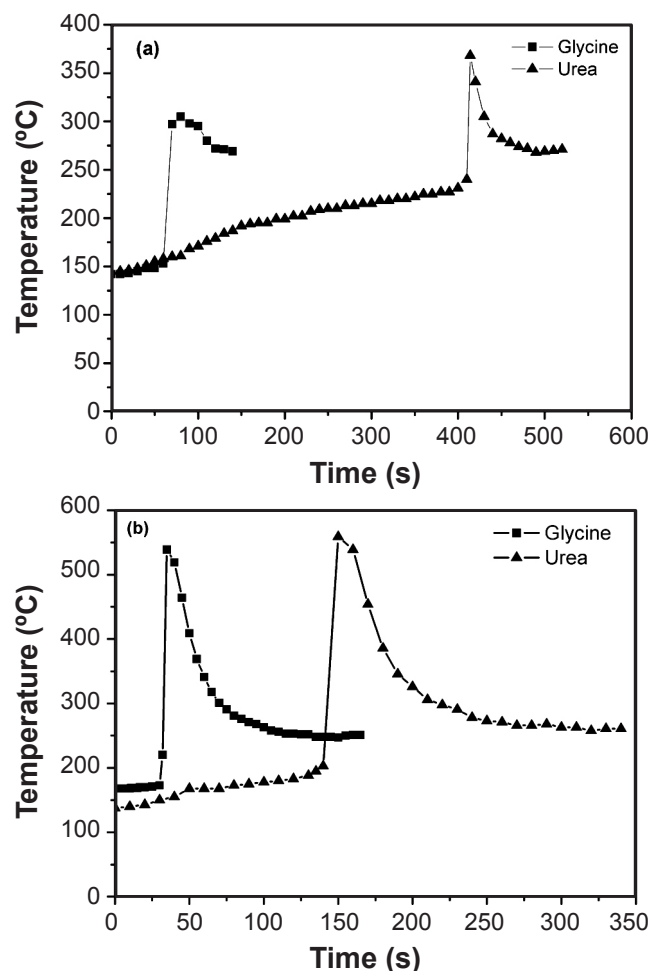


Figure 2: Evolution of temperature as a function of time during combustion synthesis for (a) LSM and (b) LSC powders. [Figura 2: Evolução da temperatura com o tempo durante a síntese por combustão dos pós de (a) LSM e (b) LSC.]

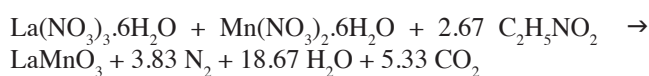
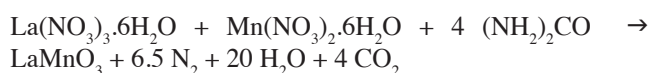
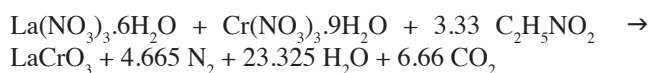
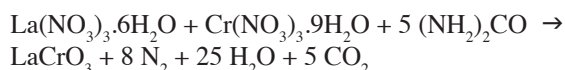
Deshpande *et al.* [18] measured a maximum reaction temperature of 806 °C for LSC prepared by combustion with glycine, and the complete conversion occurred in only 10 s, when using a fuel/oxidizer ratio between 0.7 and 1.2. The temperatures measured in the present study (with fuel/oxidizer ratio =1) were lower than those reported by Deshpande *et al.* [18], which can be related to inhomogeneous precursor mixture and higher dissipation of heat, with a longer time of reaction. On the other hand, Civera *et al.* [29] observed no visible reaction during combustion synthesis of LaMnO₃ using stoichiometric conditions with urea. Thus, the measurement of the combustion temperature is highly sensitive to the specific conditions employed by each group.

The combustion process with glycine is much more violent and faster, leading to an incomplete combustion, with large amount of organic residues, and formation of an aggregate structure, as will be shown later. Hwang *et al.* [30] showed that glycine has a higher melting point and its heat of combustion is more negative than urea, which may be contributing for the incomplete combustion when glycine was used as fuel in this work.

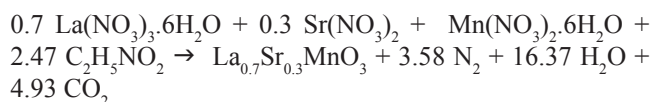
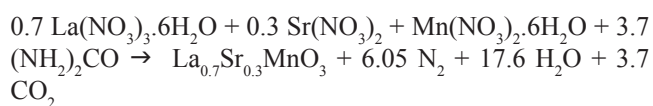
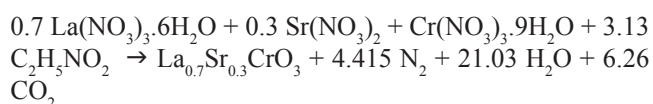
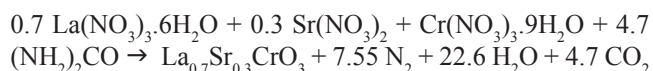
Thermodynamic calculations

According to the principle of propellant chemistry and considering that N₂, CO₂ and H₂O are the main gaseous products evolved, the combustion reactions of each process can be expressed as follows:

Non-doped samples:



Doped samples:



The enthalpies of combustion for each reaction previously described, as well as the adiabatic flame temperatures, are shown in Table I. All combustion reactions are exothermic and supply the heat needed for the synthesis reaction. The adiabatic flame temperatures are supposed high enough to promote the perovskite synthesis. As expected, the measured combustion temperatures (Table I) are lower than the theoretically calculated values due to radiative losses, heating of air, and incomplete combustion of the reaction mixture [22].

Table I - Maximum combustion temperature, enthalpy of combustion and adiabatic flame temperature for each sample.

[Tabela I - Microdeformação (ϵ), tamanho médio de cristalito (D_{XRD}) e parâmetros de rede das amostras calcinadas.]

Sample	Maximum combustion temperature (°C)	ΔH^0 (kcal.mol ⁻¹)	Adiabatic flame temperature (°C)
LMU	343	- 3.3	547
LMG	535	- 26.5	627
LCU	469	- 178.5	957
LCG	504	- 216.7	1125
LSMU	369	- 2.8	624
LSMG	303	- 34.7	679
LSCU	557	- 115.7	955
LSCG	537	- 152.8	1048

According to Table I, the calculated values of heat of combustion and adiabatic flame temperatures for perovskites synthesized with glycine are higher than those derived from urea route. In spite of this, the combustion reaction remains incomplete in the glycine route, with large amount of organic residues, as will be shown by TGA profiles. This may be attributed to inhomogeneous precursor mixture forming an unstable gel. In such case, the combustion heat can be dissipated to the surrounding colder region where fuel/oxidant rate is not favorable for combustion and consequently the flame temperature would come down [31].

Phase formation and microstructure

XRD patterns of the non-doped samples are shown in Fig. 3. Before calcination (Fig. 3a) there was formation of a great number of secondary phases for chromite samples, mainly chromium oxides. For manganites, perovskite phase was formed for LMU sample, while LMG was almost amorphous. Thus, the high temperature achieved during combustion reaction is not enough to promote perovskite formation, probably because the time of reaction is too short. After calcination (Fig. 3b), there was a good crystallization of LaMnO₃ (ICSD 470373) and LaCrO₃ (JCPDS 241016) phases, with only a small formation of secondary phase for LCG sample.

Fig. 4 shows the XRD patterns of doped perovskites. Before calcination (Fig. 4a) there was also formation of a great number of secondary phases, mainly for manganite samples. After calcination (Fig. 4b) the presence of secondary phases decreased significantly, showing that calcination is an essential step for a good crystallization of perovskite phase. This result agrees with Muskasyan *et al.* [17] who pointed out the need of a calcination step for the as-synthesized LSC powders, in order to remove residual

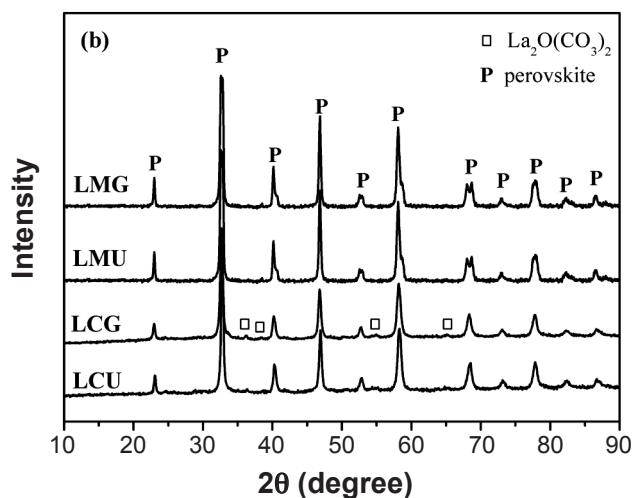
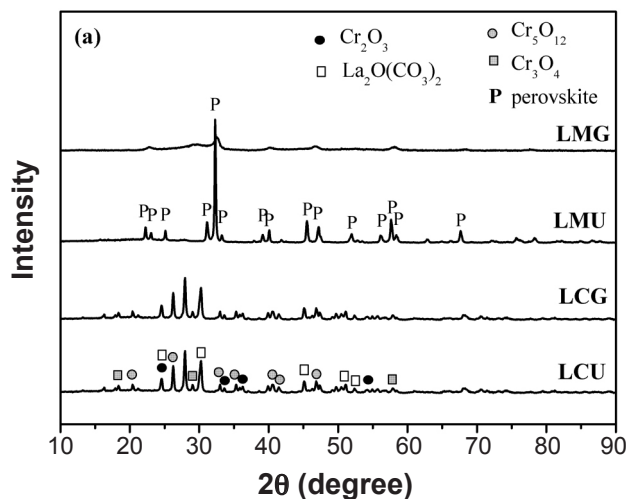


Figure 3: XRD patterns of the non-doped perovskite powders before (a) and after (b) calcination.

[Figura 3: Padrão de difração das perovskitas não dopadas antes (a) e depois (b) da calcinação.]

water and other volatile components and to improve crystalline structure of the powder.

For doped manganite samples, the combustion reaction with urea is far more complete, resulting in a crystalline material with single LSM phase (ICSD 473444). When manganite was prepared using glycine there was formation of secondary phases of SrCO_3 (JCPDS 50418) and SrMnO_3 (JCPDS 241221), because of incomplete combustion reaction. The formation of carbonate may be due to reaction between SrO and CO_2 decomposed from organic compounds during the combustion reaction [14, 32]. For doped chromites, there was only formation of LSC phase (JCPDS 321240) when using urea and a small contribution of SrCrO_4 phase (JCPDS 350743) for the sample derived from glycine route. The higher temperatures achieved during combustion synthesis of chromites (Table I) contribute to a good phase formation, practically without secondary phases.

Table II shows the microstrain and crystallite sizes calculated from XRD data using the Williamson-Hall

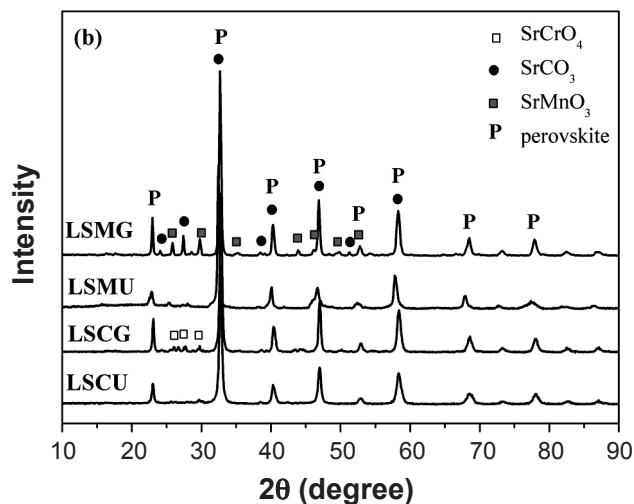
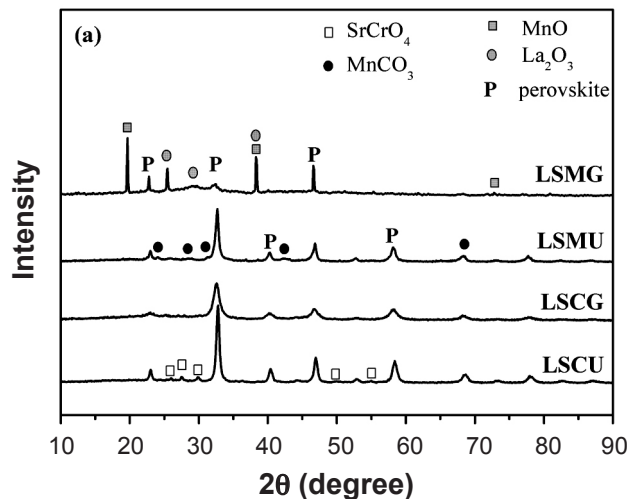


Figure 4: XRD patterns of the doped perovskite powders before (a) and after (b) calcination.

[Figura 4: Padrão de difração das perovskitas dopadas antes (a) e depois (b) da calcinação.]

equation, and the lattice parameters.

All products obtained in this work were nanocrystalline with sizes ranging between 19.5 and 24.9 nm. Broad XRD peaks indicate the nanocrystalline nature of the synthesized powders and not lattice distortions, since the values of microstrain are very low. The crystallite sizes are close to that reported by Berger *et al.* [15] for LSM synthesized by combustion with glycine (19 nm). According to Pingbo *et al.* [16], the crystallite size of LSM increased from 20 nm to 80 nm when glycine/ NO_3^- ratio decreased from 1.1 to 0.8. It is worth noting that the crystallite sizes obtained by the combustion method are much smaller than those obtained by other methods, as reported by Rida *et al.* [33] for LaCrO_3 prepared by sol-gel synthesis and calcined at 800 °C (179 nm).

For both manganite and chromite, smaller crystallite sizes were formed when using urea because the large volume of gases evolved enhances dissipation of heat and limits the inter-particle contact [34]. The lattice parameters calculated

Table II - Microstrain (ϵ), average crystallite size (D_{XRD}) and lattice parameters of the calcined samples.[Tabela II - Microdeformação (ϵ), tamanho médio de cristalito (D_{XRD}) e parâmetros de rede das amostras calcinadas.]

Sample	ϵ (%)	D_{XRD} (nm)	Lattice parameters (\AA)
LMU	0.32	20.0	a= 5.4344; b= 5.5073; c= 7.7500*
LMG	0.42	22.4	a= 5.5110; b= 5.5429; c= 7.7152*
LCU	0.23	19.5	a= 5.4655; b= 5.4934; c= 7.7462**
LCG	0.27	22.3	a= 5.4915; b= 5.5186; c= 7.7074**
LSMU	0.54	20.9	a= 5.4875; c= 13.4279***
LSMG	0.20	22.6	a= 5.5012; c= 13.3630***
LSCU	0.38	23.2	a= 5.4545; c= 13.4174****
LSCG	0.24	24.9	a= 5.6013; c= 13.3049****

Theoretical cell parameters: * ICSD 470373 (a= 5.5311; b=5.4943; c=7.7814 \AA); ** JCPDS 241016 (a=5.4790; b=5.5130; c= 7.7560 \AA); ***ICSD 473444 a)=473444 (a=5.4953; c=13.3422 \AA); ****JCPDS 321240 (a=5.4030; c= 13.3010 \AA)

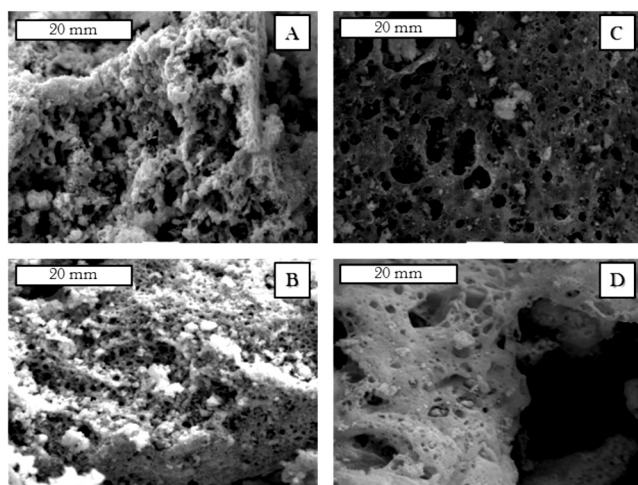


Figure 5: Micrographs of the samples: (A) LSCU; (B) LSMU; (C) LSCG and (D) LSMG.

[Figura 5: Micrografias das amostras: (A) LSCU; (B) LSMU; (C) LSCG e (D) LSMG.]

from XRD data are consistent with the orthorhombic structure for non-doped samples and rhombohedral structure for doped perovskites, in agreement with other literature data [15, 35].

Fig. 5 shows SEM micrographs of the doped perovskite samples after calcination. The powders presented a spongy aspect, with primary particles linked together in agglomerates of different sizes and shapes, in accordance with other results of combustion synthesis in the literature [15, 17, 34]. The samples prepared with urea have higher porosity compared with glycine. The combustion reaction with urea presents a great evolution of gases, resulting in porous structures with smaller particle size.

Thermal analysis

Fig. 6 shows TGA curves of the as-synthesized powders. Thermal decomposition takes place in different stages, depending on the fuel, and burn out of organics is complete

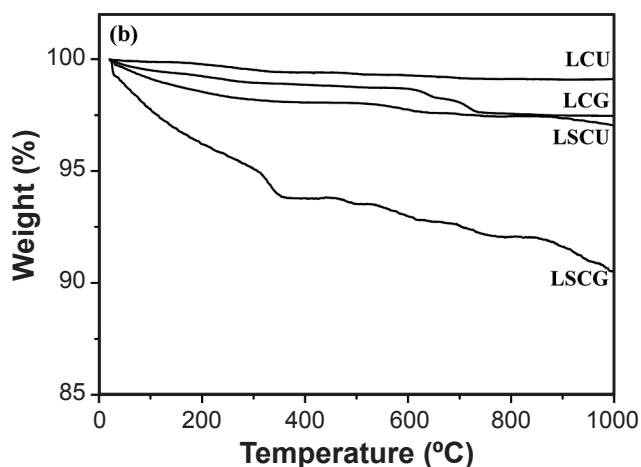
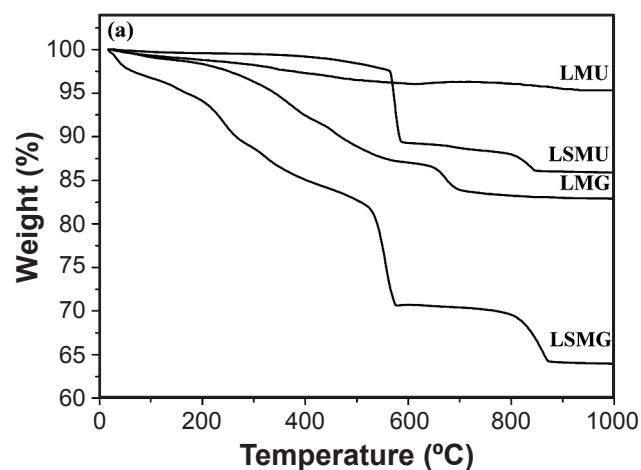


Figure 6: TGA curves of the as-synthesized manganite (a) and chromite (b) samples.

[Figura 6: Curvas de TG das amostras recém preparadas: manganitas (a) e cromitas (b).]

at about 850-900 °C for manganites and 1000 °C for chromites. All non-doped samples presented lower weight loss than the doped ones. For manganite samples, two or three decomposition stages can be clearly distinguished:

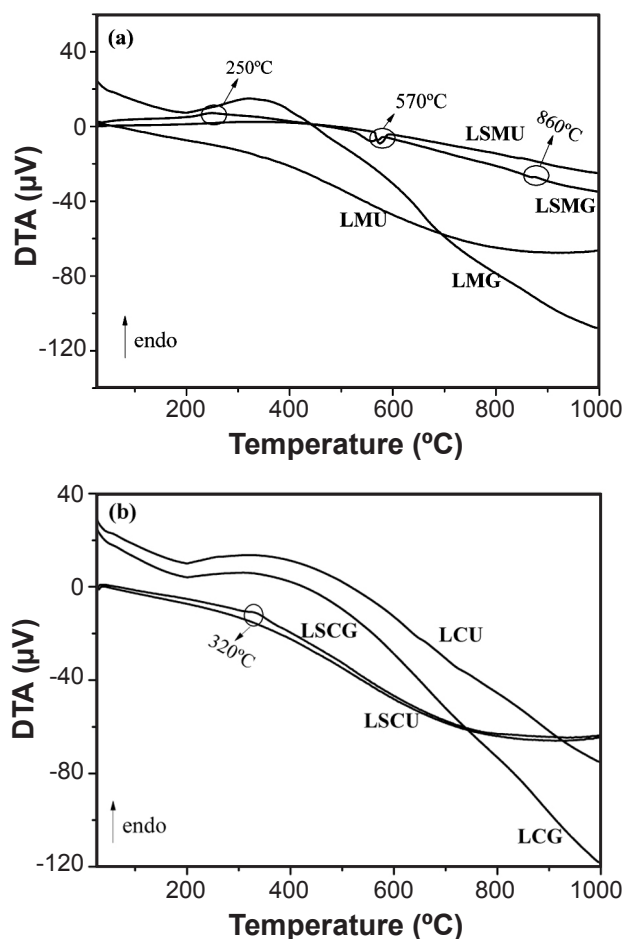


Figure 7: DTA curves of the as-synthesized manganite (a) and chromite (b) samples.

[Figura 7: Curvas de ATD das amostras recém preparadas: manganitas (a) e cromitas (b).]

the first, at 200 °C, can be assigned to the desorption of physisorbed water; the second, at 550-600 °C, can be associated with the oxidation of combustion residues, mainly fuel that was not burnt during the fast combustion reaction; the third, at 850 °C, may be due to complete dissociation of carbonates produced during combustion and formation of LSM phase [34, 36]. For chromite samples it is difficult to distinguish between decomposition stages, with a slightly continuous weight loss. It is worth noting that the weight loss for the samples prepared using glycine is always higher than those derived from urea, which is directly related to the incomplete combustion in the glycine route.

DTA profiles are displayed in Fig. 7. For manganite samples, doping causes a significant change in DTA curves. They show a small endothermic peak at 250 °C for LSMG sample, associated with loss of adsorbed water, a great exothermic peak at 570 °C, due to combustion of organic residues, and a small endothermic one at 860 °C, due to carbonate dissociation and formation of LSM [36]. DTA curve of LSCG exhibits only a small endothermic peak at 320 °C, related to the decomposition of hydroxy species

formed by reaction between glycine and nitrate anions [15].

CONCLUSIONS

The combustion synthesis method from nitrate precursors has been used to prepare nanocrystalline doped and non-doped lanthanum manganite and chromite powders. According to our results, combustion temperature, phase formation, crystallite size, porosity and thermal stability are dependent on the nature of the fuel (urea or glycine). All these properties should be considered together when preparing an electrode or interconnect for SOFCs. The high values of adiabatic flame temperatures theoretically calculated suggest favorable conditions for combustion; however, calcination is required in order to obtain good crystallization of perovskite phase. The combustion temperatures experimentally measured are far below the adiabatic flame temperatures due to a great dissipation of heat and incomplete combustion. The combustion reaction with urea is slower, with evolution of a large amount of gases, resulting in particles with only one crystalline phase, smaller crystallites and higher porosity. The combustion reaction using glycine is violent and remains localized and incomplete, justifying the formation of secondary phases even after calcination and a large weight loss observed in TGA curves due to organic residues. Thus, the combustion method using urea as propellant is a suitable route to synthesize perovskite materials. This technique is presented as a rapid and economical alternative for preparation of ceramic materials used as electrodes and interconnects in SOFC.

ACKNOWLEDGEMENTS

The authors thank CNPq, CAPES and FAPERJ for financial support granted to carry out this work.

REFERENCES

- [1] H. Tanaka, M. Misono, *Curr. Opin. Solid State Mater. Sci.* **5** (2001) 381.
- [2] D. Z. de Florio, F. C. Fonseca, E. N. S. Muccillo, R. Muccillo, *Cerâmica* **50**, 316 (2004) 275.
- [3] S. C. Singhal, K. Kendall, *High Temperature Solid Oxide Fuel Cells: Fundamentals, Design and Applications*, Elsevier, Oxford, England (2004).
- [4] S. P. Jiang, J. Li, *Cathodes*, in: J. W. Fergus, R. Hui, J. Li, D. P. Wilkinson, J. Zhang, Eds., *Solid Oxide Fuel Cells: Materials, Properties and Performance*, CRC Press (2009) pp. 131-177.
- [5] Q. Zhang, T. Nakagawa, F. Saito, *J. Alloys Comp.* **308** (2000) 121.
- [6] R. J. Bell, G. J. Millar, J. Drennan, *Solid State Ionics* **131** (2000) 211.
- [7] L. A. Chick, L. R. Pederson, G. D. Maupin, J. L. Bates, L. E. Thomas, G. J. Exarhos, *Mater. Lett.* **10** (1990) 6.
- [8] Y. J. Yang, T. -L. Wen, H. Tu, D. -Q. Wang, J. Yang, *Solid*

State Ionics **135** (2000) 475.

[9] K. C. Patil, S. T. Aruna, T. Mimani, *Curr. Opinion Solid State Mater. Sci.* **6** (2002) 507.

[10] A. Varma, A. S. Rogachev, A. S. Mukasyan, S. Hwang, *Adv. Chem. Eng.* **24** (1998) 79.

[11] A. M. Segadães, M. R. Morelli, R. G. A. Kiminami, J. Eur. Ceram. Soc. **18** (1988) 771.

[12] D. A. Fumo, J. R. Jurado, A. M. Segadães, J. R. Frade, *Mater. Res. Bull.* **32** (1997) 1459.

[13] K. Prabhakaran, J. Joseph, N. M. Gokhale, S. C. Sharma, R. Lal, *Ceram. Int.* **31** (2005) 327.

[14] R. S. Guo, Q. T. Wei, H. L. Li, F. H. Wang, *Mater. Lett.* **60** (2006) 261.

[15] D. Berger, C. Matei, F. Papa, D. Macovei, V. Fruth, J. P. Deloume, *J. Eur. Ceram. Soc.* **27** (2007) 4395.

[16] X. Pingbo, Z. Weiping, Y. Kuo, J. Long, Z. Weiwei, X. Shangda, *J. Alloys Comp.* **90** (2000) 90.

[17] A. S. Mukasyan, C. Costello, K. P. Sherlock, D. Lafarga, A. Varma, *Sep. Purif. Technol.* **25** (2001) 117.

[18] K. Deshpande, A. Mukasyan, A. Varma, *J. Am. Ceram. Soc.* **86** (2003) 1149.

[19] S. Biamino, C. Badini, *J. Eur. Ceram. Soc.* **24** (2004) 3021.

[20] A. Ringuedé, J. A. Labrincha, J. R. Frade, *Solid State Ionics* **141-142** (2001) 549.

[21] J. A. Dean, Ed., *Lange's Handbook of Chemistry*, McGraw Hill, New York, USA (1979).

[22] R. D. Purohit, B. P. Sharma, K. T. Pillai, A. K. Tyagi, *Mater. Res. Bull.* **36** (2001) 2711.

[23] J. Cheng, A. Navrotsky, *J. Solid State Chem.* **178** (2005) 234.

[24] C. Zhanheng, X. Xianran, Y. Wenxia, H. Xiaowei, L. Hongwei, *Rare Metals* **25** (2006) 562.

[25] H. Yokokawa, N. Sakai, T. Kawada, M. Dokiya, *J. Electrochem. Soc.* **138** (1991) 1018.

[26] J. Sfeir, *J. Power Sources* **118** (2003) 276.

[27] G. K. Williamson, W. H. Hall, *Acta Metallurgica* **1** (1953) 22.

[28] L. Conceição, N. F. P. Ribeiro, J. G. M. Furtado, M. M. V. M. Souza, *Ceram. Int.* **35** (2009) 1683.

[29] A. Civera, M. Pavese, G. Saracco, V. Specchia, *Catal. Today* **83** (2003) 199.

[30] C.-C. Hwang, T.-Y. Wu, J. Wan, J.-S. Tsai, *Mater. Sci. Eng. B* **111**(2004) 49.

[31] R. K. Lenka, T. Mahata, P. K. Sinha, A. K. Tyagi, *J. Alloys Comp.* **466** (2008) 326.

[32] N. M. Nagabhushana, R. P. S. Chakradhar, K. P. Ramesh, C. Shivakumara, G. T. Chandrappa, *Mater. Res. Bull.* **41** (2006) 1735.

[33] K. Rida, A. Benabbas, F. Bouremmad, M. A. Peña, E. Sastre, A. Martínez-Arias, *Appl. Catal. A* **327** (2007) 173.

[34] N. P. Bansal, Z. Zhong, *J. Power Sources* **158** (2006) 148.

[35] M. Mori, Y. Hiei, N. M. Sammes, *Solid State Ionics* **123** (1999) 103.

[36] A. Ghosh, A. K. Sahu, A. K. Gulnar, A. K. Suri, *Scripta Mater.* **52** (2005) 1305.

(*Rec. 14/12/2011, Rev. 08/02/2012, Ac. 09/02/2012*)